Korean J. Chem. Eng., **31**(11), 1911-1918 (2014)
DOI: 10.1007/s11814-014-0206-0
pISSN: 0256-1115
eISSN: 1975-7220

REVIEW PAPER

Biosorption mechanism of Zn^{2+} from aqueous solution by spent substrates of pleurotus ostreatus

XiaoJing Hu*, LiLong Yan*, Haidong Gu*, TingTing Zang*, Yu Jin, and JuanJuan Qu*,†**

*College of Resources and Environment, Northeast Agricultural University, Harbin 150030, China
**State Key Laboratory of Urban Water Resource and Environment, Harbin Institute of Technology, Harbin 150090, China
(*Received 9 November 2013 • accepted 22 July 2014*)

Abstract−To solve the problem of heavy metal pollution and agricultural wastes reclamation, spent substrate of pleurotus ostreatus (SSPO) was used as adsorbent to remove Zn^{2+} from aqueous solution. The biosorption of zinc ions on SSPO was studied as a function of the solution pH, temperature and initial Zn^{2+} concentration. The equilibrium sorption data were well represented by linear Langmuir isotherm models with R^2 value of 0.9955 and non-linear Freundlich with R^2 value of 0.9973. The BET surface area of SSPO can reach 51.16 m^2g^{-1}. SEM-EDX and XRD revealed that $(NH_4)_2Zn\cdot H_2O$ and $Zn_2PO_4(OH)$ were the main compounds in metal-loaded SSPO. FTIR analysis indicated the governing functional groups such as O-H, N-H and P=O played an important role in biosorption. The desorption studies showed the reversibility of SSPO. The results indicate that SSPO is a potential adsorbent in wastewater treatment due to its great sorption capacity and low cost.

Keywords: SSPO, Zinc Ions, Isotherm Model, Biosorption Mechanism

INTRODUCTION

Heavy metal pollution along with the rapid industrial development has increasingly become a serious environmental challenge for China. Zinc, one of the micronutrient elements for human health, has often been found in effluents from mining, electroplating, metallurgy, refining, alloy etc. It cannot be biodegraded but accumulates in organisms through the food chain. Excessive ingestion of zinc may bring about a series of physiological dysfunctions such as depression, lethargy, simple osteoporosis, brain tissue atrophy, kidney and pancreas damage [1,2].

Chemical precipitation, ion-exchange, reverse osmosis, oxidation reduction and coagulation are conventional methods generally used for the removal of zinc ions from effluents. However, there are many disadvantages such as high cost, large energy consumption, complicated operation, high energy input and poor treatment efficiency at low metal concentration [3,4].

Compared with the conventional methods, biosorption shows its superiority in cost-effectiveness, non-pollution, high efficiency, wide adaptability and stable performance in the treatment of low metal ion concentration effluents [5]. Recently, attention has been increasingly focused on agriculture and food industry wastes, which are used as adsorbent to bind the heavy metals from dilute solution, such as orange peel, sawdust, rice husk, and discard mycelium [6-8].

China is the largest producer of edible fungus in the world with a nationwide yield of around 31,000,000 tons in 2012, resulting in about 50,000,000 tons spent substrate. Around the country, Heilongjiang is one of the main producing areas of edible mushroom. Except for some spent wastes used for cultivation substrates, millions of tons of the spent are discarded or burned on the spot, which has contaminated environment and squandered resources [9]. The spent substrate is a mixture of lignocelluloses and mycelium. Thus, this biomaterial contains plenty of cellulose, hemicelluloses, lignin, chitin, carbohydrate and organic acids. Abundant function groups such as hydroxyl, carbonyl, carboxyl, amino and phosphate groups on the surface of this biomass, can chelate heavy metal cations in aqueous solution. Numerous studies have been published on biosorption of heavy metal ions with agriculture wastes or mycelium, and the effects are comparatively obvious [10-12]. But few reports refer to SSPO (the spent substrates of pleurotus ostreatus). In this study, SSPO were regarded as potential adsorbent without chemical modification for the treatment of simulated wastewater containing zinc ions. The characteristics of the biomass were discussed. Langmuir and Freundlich isotherm models were applied to evaluate the sorption phenomenon. Furthermore, BET, SEM-EDX, FTIR and XRD were employed to preliminarily explore the biosorption mechanism.

MATERIALS AND METHODS

1. Preparation of the Biosorbents

SSPO flotsam was kindly provided by Wood Edible Fungi Plants, Harbin, China. The biomass was rinsed with distilled water and oven-dried at 60±1 °C for a period of 12 h till constant weight followed by grinding and 40 mesh sieving, then they were autoclaved and stored for use.

The standard stock solution of Zn^{2+} (10 $g\cdot L^{-1}$) was obtained by dissolving appropriate amount of zinc nitrate hexahydrate ($Zn(NO_3)_2\cdot 6H_2O$) in deionized water. Different concentrations of zinc ions were provided by suitable dilution of the stock solution in following experiments. All chemicals employed were analytical grade. After each experiment, the suspensions were filtered and the residual metal ions concentrations were determined by atomic absorption spectro-

†To whom correspondence should be addressed.
E-mail: juanjuan4050234@163.com

photometer (AAS) (SHIMADZU, JAPAN).

2. Batch Biosorption Experiments

Batch experiments were conducted at ambient temperature (25± 1 °C) in 150 mL Erlenmeyer flasks containing 100 mL diluted zinc ions solution, which were stirred at 150 rpm on a thermostatic rotary shaker. Fixed quantity of biomass (0.1 g) was added to each flask, which was set in our previous experiments. To study the effect of pH on metal removal by SSPO, 0.1 M of HNO_3 or NaOH was gradually added to adjust pH value from 2 to 8 with the constant of above-mentioned conditions and the final pH of reaction solution was detected. Contact temperature and initial concentration of zinc ions were varied from 5 °C to 40 °C and 25 to 200 mg·L^{-1}, respectively.

All the biosorption experiments were performed in triplicate and the average values were used in data analysis. The efficiency of biosorption (R) and the adsorption capacity of biomass (Q) at equilibrium were calculated using the following equations:

$$R = \frac{(C_j - C_e)}{C_j} \times 100\%$$

$$Q = \frac{(C_j - C_e)V}{m}$$

where C_j and C_e are the initial and equilibrium concentration of zinc ions solution, respectively (mg·L^{-1}), V is the volume of reaction solutions (we unified them for 100 mL) (mL), m is the dried mass of biosorbent in the reaction solution (g).

3. Desorption Procedure

The desorption of zinc ions from the biomass was studied at ambient temperature (25±1 °C) with 0.1 g metal loaded biomass into 100 ml 0.1 M HCl. After each experiment, the suspensions were filtered and the residual zinc ions concentrations were determined by atomic absorption spectrophotometer. The biosorption-desorption cycles were repeated five times under the same conditions. Desorption efficiency was calculated by using the following equation:

$$\text{Desorption efficiency } (\%) = \frac{\text{amount of zinc ions desorbed}}{\text{initially sorbed zinc ions}} \times 100\%$$

4. Determination of pH_{zpc}

The pH_{zpc} was determined with a method previously described by Rivera et al. Fifty (50) ml of 0.01 M NaCl solution was placed in an Erlenmeyer flask. The initial pH values of solutions were adjusted to 2-8 with 0.1 M HNO_3 and NaOH solutions. 0.1 g biomass was added to each flask, stirred and the final pH determined after 24 h. The pH_{zpc} was the point where the curve crossed the line $pH_{initial}$-pH_{final} and was taken as the point of zero charge [13].

5. Biosorption Mechanism

Native and metal-loaded SSPO were respectively weighed and dried on 60±1 °C for 24 h. Their surface morphology and composition of elements were examined with a scanning electron microscope (QUANTA200, USA) equipped with energy disperse X-ray analysis. The samples were coated with aurum by a vacuum electric sputter coater. The textural properties of SSPO were determined using surface area and porosity analyzer (ASAP2020 USA).

Then, Fourier transform infrared spectrometry (FTIR) (ALPHA-T, GERMANY) was applied to acquire the infrared spectra of the pristine and metal-loaded SSPO to investigate the acting functional groups present in the adsorbents. 1 mg of finely triturated powder specimens was encapsulated in 100 mg of IR grade KBr to prepare the translucent sample disks (the proportion of SSPO and KBr is approximately 1 : 100). The wave number ranged from 4,000 cm^{-1} to 400 cm^{-1}.

Subsequently, X-ray diffractograms of the oven-dried adsorbent before and after zinc loading were recorded on an X-ray diffraction spectrometer (D/max2200, JAPAN), by Zn$K\alpha$, at 40 kV and 30 mA with a scan rate of 4°·min^{-1} and an interpolated step of 0.02° in the 2θ range from 5° to 80°.

RESULTS AND DISCUSSION

1. pH_{zpc} and Effect of Solution pH

When the solid surface is net electrical neutral, the pH value of the aqueous solution is considered as pH_{zpc}, a very important characteristic that determines the pH. Cation adsorption will be more favorable at pH value higher than pH_{zpc} [14]. The value of pH_{zpc} (5.98) was close to the value of pH for SSPO in aqueous solution (6.12).

It is well known that the pH value is a key parameter for biosorption of metal ions in aqueous solutions. The effect of pH on Zn^{2+} removal was studied in the range of 2-8 at 25 °C for 60 min in this research. As shown in Fig. 1, the biosorption capacity was so low that the uptake of ionic zinc was just about 3.68 mg·g^{-1} as initial solution pH was 2. The absorbed metal ions per unit weight of biosorbents increased gradually when the pH values increased from 2 to 8. The final pH values of 2, 3, 4 are consistent with the initial that the initial pH values of 5, 6, 7 and 8 approximately fluctuated from 6 to 7 over time, and the biosorption capacity of SSPO changed little after pH 5. Thus, the maximum of sorption capacity took place at around pH 6 and 7 during the adsorption process.

The dependence of metal extractability on pH is related to both the surface functional groups on the biomass and the metal chemistry in solution [15]. At pH value lower than 3 in this research, the competition was so intensive for active sites between hydrogen and zinc ions that metal ion removal was inhibited. Apparent preponderance of hydrogen ions impeded the approach of zinc ions as a result of repulsive force. The density of negative charges would be increased on the adsorbent surface, when effective groups such as

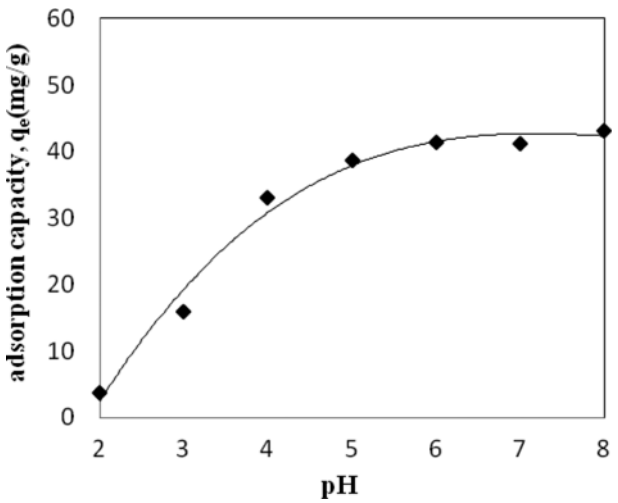

Fig. 1. Effect of solution pH on zinc biosorption (temperature=25 °C, biomass dosage=1 g·L^{-1}, contact time=60 min, zinc initial concentration=100 mg·L^{-1}).

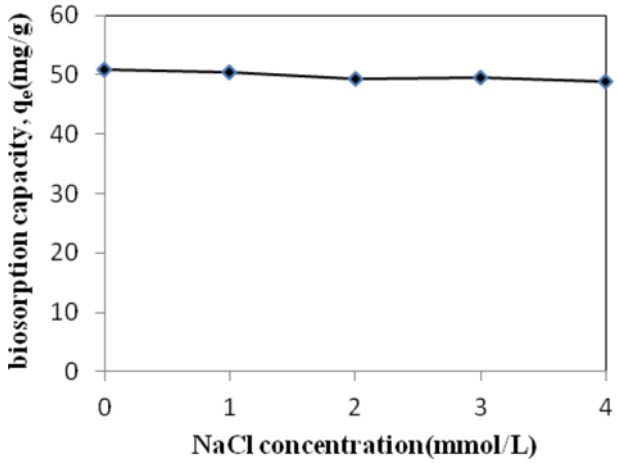

Fig. 2. Effect of ionic strength on the Zn^{2+} biosorption (temperature =25 °C, biomass dosage=1 g·L^{-1}, contact time=60 min, zinc initial concentration=100 mg·L^{-1}).

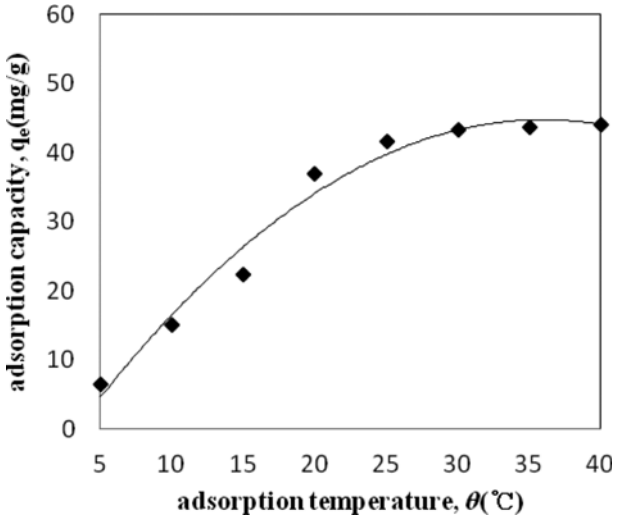

Fig. 3. Effect of zinc adsorption temperature (pH=6, biomass dosage=1 g·L^{-1}, contact time=60 min, zinc initial concentration =100 mg·L^{-1}).

carboxylate and hydroxyl groups were exposed as the pH increased, which in turn increased the attraction of metallic ions with positive charge and allowed the biosorption onto the biomass surface [16]. But higher pH could bring out the formation of $Zn(OH)^+$ or $Zn(OH)_2$, which resulted in a reduction of the adsorption capacity, due to the diminution of the formal charge of the zinc ions [17]. Moreover, acidification was required to prevent the formation of polynuclear hydroxo-bridged species or the precipitation of basic salts [18]. All of the following adsorption experiments were conducted at this favorable pH value.

2. Effect of Ionic Strength (IS)

Effect of ionic strength on Zn^{2+} biosorption was investigated by previous experiments at different concentrations of NaCl (0-4.0 mmol/L) described in Fig. 2. The ionic strength can be explained as existing competition of Na^+ ions with heavy metal for the adsorption site that takes place with the concentration increase of Na^+ in aqueous solution. So the degree of dissociation of the molecules was also increased due to the facilitation of protonation caused by salts and the adsorption was sensitive to the change in ionic strength if electrostatic attraction played a role in the biosorption [19]. That is, at high ionic strength, the increased amount of NaCl can help to swamp the surface of the biomass which is bound to be surrounded by an electrical diffused double layer [20]. But in biosorption of Zn^{2+} on SSPO, with the increase of the ionic strength, the biosorption capacity slightly changed. So the ionic strength had little effect on the biosorption. As shown in Fig. 2, ionic strength only had a slight effect on Zn^{2+} biosorption by SSPO at low metal concentration regardless of NaCl concentration. In short, the influence of ionic strength on Zn^{2+} biosorption is negligible for SSPO.

3. Effect of Adsorption Temperature

To evaluate the effect of temperature on adsorbed Zn^{2+} amount by SSPO, experiments were performed in the range of 5-40 °C at pH 6 for 60 min. Fig. 3 illustrates that the adsorption capacity of Zn^{2+} on SSPO was favored at higher temperatures at an initial Zn^{2+} concentration of 100 mg·L^{-1}. The figure demonstrates that the amount of Zn^{2+} removed by SSPO varied from 6.43 mg·g^{-1} to 44.01 mg·g^{-1} with the temperature ranging from 5 °C to 40 °C. It was favorable for intraparticle transmission and occurrence of chemisorption at higher temperature. Besides, the increase of biosorption capacity with temperature may be attributed to either increase in the number of available active sites for biosorption due to bond rupture or decrease in the thickness of the boundary layer surrounding the biosorbents [21]. The change of adsorption capacity indicated the adsorption process was affected significantly by the temperature. In practice, as the temperature increased, greater energy was consumed. In addition, the biosorption capacity of zinc ions was basically constant over 30 °C as seen in Fig. 2. Furthermore, according to climate of Heilongjiang, the most northeast province in China, 30 °C was chosen as the optimum temperature.

4. Effect of Zn^{2+} Initial Concentration

Experiments were conducted to investigate the effect of the initial Zn^{2+} concentration, which was adjusted to the range of 25-200 mg·L^{-1} under optimal pH and contact temperature. Fig. 4 shows that metal uptake increased with initial zinc ion concentration increas-

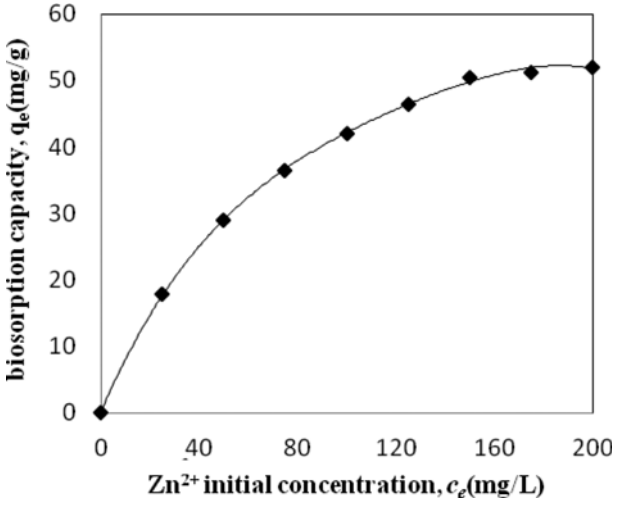

Fig. 4. Effect of zinc initial concentration (pH=6, temperature= 25 °C, biomass dosage=1 g·L^{-1}, contact time=60 min).

ing at constant solution volume and biomass dosage. The increase leveling off after the concentration exceeded 150 mg·L^{-1} may be due to the lack of adequate active sites to accommodate much more metal ions in the solution when biomass became saturated. Furthermore, the increase of metal uptake was a result of the increase in the driving force, i.e., concentration gradient to conquer transmission resistance [22]. Hence, metal ion removal was strongly dependent on initial metal concentration.

5. Biosorption Isotherm Model

Langmuir and Freundlich models are widely employed in equilibrium experiments to elaborate the adsorption mechanisms. The Langmuir model considers sorption by monolayer type and supposes that all the active sites on the sorbent surface have the same affinity to the sorbate [23]. The adsorption capacity achieves a maximum when adsorbent sites saturate. The rates of adsorption and desorption become the same when dynamic equilibrium arrives. The familiar form of the Langmuir isotherm is expressed as follows [24]:

$$\frac{C_e}{q_e} = \frac{C_e}{q_{max}} + \frac{1}{K_L q_{max}}$$

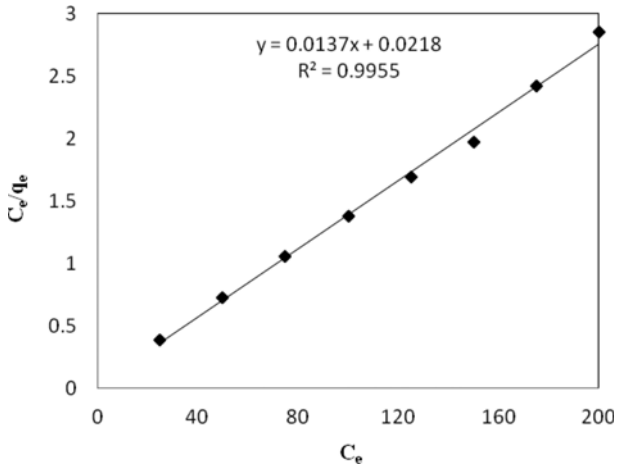

Fig. 5. Langmuir adsorption isotherm for biosorption of Zn^{2+} (pH =6, temperature=30 °C, biomass dosage=1 g·L^{-1}, contact time=60 min).

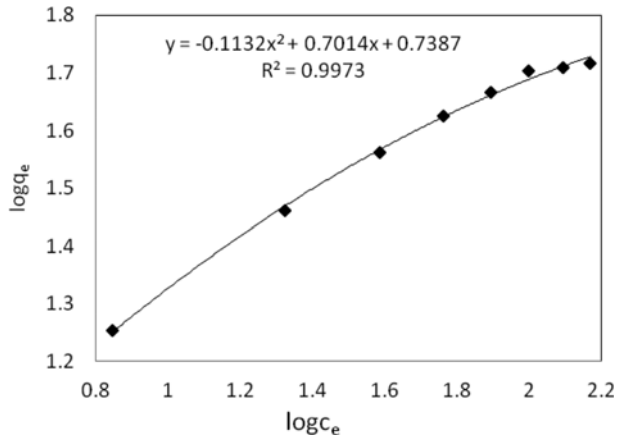

Fig. 6. Freundlich adsorption isotherm for biosorption of Zn^{2+} (pH =6, temperature=30 °C, biomass dosage=1 g·L^{-1}, contact time=60 min).

where q_e is the equilibrium adsorption capacity (mg·g^{-1}), q_{max} is the maximum monolayer capacity on unit mass of adsorbent (mg·g^{-1}), C_e is the equilibrium concentration of zinc ions solution (mg·L^{-1}), K_L is Langmuir equilibrium constant related to affinity of the binding sites (L·mg^{-1}).

The experimental data for the adsorption of Zn^{2+} on SSPO were well fitted to Langmuir and Freundlich model, respectively, presented in Fig. 5 and Fig. 6.

It was found that Langmuir model of biosorption data was linear form from the Fig. 5, the relevant coefficient achieved 0.9955. Other similar biomass such as *Avena fatua* [25] and *Lentinus edodes* [26] also depend on chemisorption for removal of zinc ions from aqueous solution as their biosorption data also fit the Langmuir model, and the process of adsorption is mainly considered as monolayer adsorption on the surface of the adsorbent.

A further analysis of the Langmuir equation can be made on the basis of a dimensionless equilibrium parameter, i.e., R_L, also named as separation factor [27]. The equation is:

$$R_L = \frac{1}{1 + bC_j}$$

The nature of adsorption process is represented by separation factor, R_L: $0<R_L<1$ represents favorable adsorption and $R_L>1$ represents unfavorable adsorption; while $R_L=1$ represents reversible adsorption and $R_L=0$ irreversible adsorption.

Because of $b>0$ and $C_j>0$, the value of R_L was between 0 and 1, suggesting favorable sorption of Zn^{2+} on SSPO. This indicated that SSPO effectively adsorbed Zn^{2+} under the lower adsorbent concentration.

The Freundlich isotherm is an empirical equation which applicable to the description of adsorption phenomenon in the range of medium concentration. The general Freundlich equation is calculated as follows [28]:

$$\log q_e = \log K_F + \frac{1}{n}\log C_e$$

where K_F is a Freundlich constant representing adsorption capacity (L·g^{-1}) and n is an empirical parameter describing the adsorption intensity.

It was also found that biosorption data was well described by the Freundlich model for non-linear form from Fig. 6 using the Origin software, the relevant coefficient achieved 0.9973. The Freundlich constant K_F and n for SSPO was 28.65 and 1.30, respectively. According to Muhammad et al. [29], the magnitude of the factor n is an indication of the favorability of adsorption. The value of n ranging from 1-2 indicates favorable adsorption of metal ions on the surface of biomass. The nonlinearity indicated that the entire mechanisms of biosorption of Zn^{2+} on biomass comprised more than one sorption process [30]. It also means that, for an equilibrium zinc concentration of 2.04 mg/L, each gram of SSPO can remove 50 mg of zinc under the same experimental conditions and is higher than the biosorption of edible mushrooms as Mathialagan et al. reported [31].

6. Exploration of Biosorption Mechanism

6-1. Pore Properties and Pore Size Distribution of the SSPO

The surface properties of the biomass like BET surface area, Langmuir surface area and average pore diameter were determined and

Table 1. BET characteristics of the SSPO

Surface area	BET surface area	51.155 m^2g^{-1}
	Langmuir surface area	261.004 m^2g^{-1}
Pore size	Average surface area of pores	41.467 m^2g^{-1}
	Average volume of pores	0.051 cm^3g^{-1}
	Average pore diameter	4.894 nm

presented in Table 1. The value of BET surface area of adsorbent (51.1545 m^2/g) is much higher than surface area of the sawdust powder (3.76 m^2/g) [32] and *Schizophyllum commune* fungus (3.95 m^2/g) [33]. However, without complicated pretreatment, SSPO has much smaller surface area and biosorption capacity than activated carbon (760 m^2/g, 70.15 mg/g) [34], but it is more convenient to apply in practice.

This adsorbent with average pore diameter (4V/A) of 4.894 nm (2<d<50) is classified into mesopore material according to the International Union of Pure and Applied Chemistry (IUPAC). The high value of surface area also indicates its high porosity.

6-2. SEM-EDX Analysis of Biomass

To explore the surface characteristic and zinc uptake, SEM-EDX was used to analyze surface morphology structure and elemental variations of native and metal-loaded biomass.

The surface morphology of metal-loaded SSPO was greatly different from the native one as shown in Fig. 7. A number of microcosmic holes, ravines and wrinkles were observed on the surface of SSPO which was attached with amount of mycelium. It was obvious from the SEM that there was a more distinct internal hierarchy, more loose structure and more adsorption sites exposed on the biomass than the initial case after sudden change in bulk fluidic environment. As we all know, SSPO is made up of sawdust and mycelium, sawdust is mainly made of cellulose, hemicelluloses and lignin, besides a little ash and timber extract, most of them have comparatively stronger adsorption capacity [35,36]. So the apparent nature of SSPO determines that it has a relatively large surface for biosorption.

Further evidence of the zinc ions onto SSPO came by EDX analysis. The results of EDX spectra and element composition of the biomass are shown in Fig. 7 and Table 2. After biosorption, the presence of characteristic peaks for Zn indicated that the zinc ions were adsorbed onto SSPO. The visible change of the percentage of Ca, K, N, Na and Mg in biosorbent indicated that ion-exchange probably existed in the biosorption process in addition to complexation functional groups on the biosorbent surface [37].

6-3. XRD Analysis of Adsorbents

Fig. 8(a) and (b) show the XRD diffraction patterns of SSPO before and after biosorption of Zn. There are two broad peaks centered at 2θ=15°-25°, which indicate the typical cellulose diffraction spectrum; the major broad peaks represent higher degree of cellulose crystalline structure, and the minor broad peaks mean lower degree of polysaccharide structure. The XRD spectrum of SSPO after biosorption deviated slightly and some new peaks emerged in

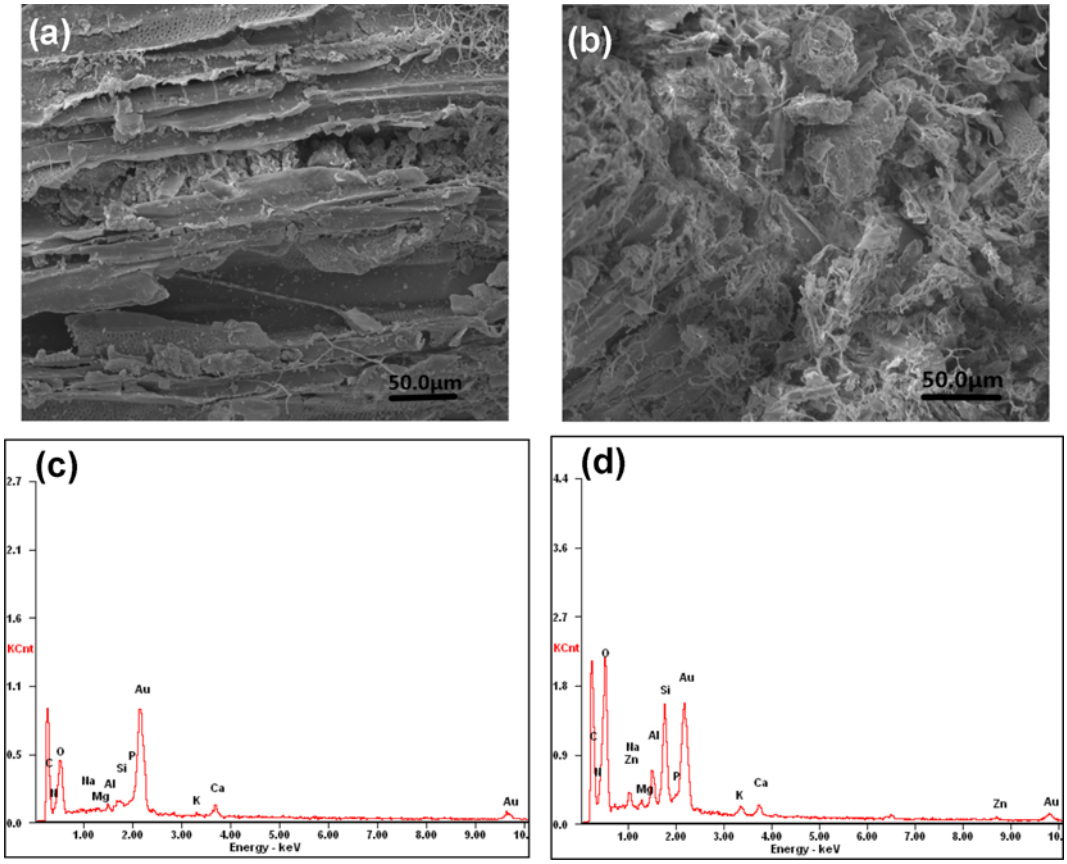

Fig. 7. SEM-EDX characterization of native (a), (c) and metal-loaded (b), (d) of SSPO (pH=6, temperature=30 °C, biomass dosage=1 g·L^{-1}, contact time=60 min, zinc initial concentration=150 mg·L^{-1}).

Table 2. Elemental composition from EDX analysis of native and metal-loaded SSPO

Element	Native SSPO	Metal-loaded SSPO
Element	Wt%	Wt%
C (%)	44.15	39.01
N (%)	16.32	15.47
O (%)	27.28	29.79
Na (%)	n.d.	00.23
Mg (%)	00.80	00.34
Al (%)	00.73	01.98
Si (%)	01.58	06.28
P (%)	01.76	01.08
K (%)	01.10	01.05
Ca (%)	03.95	01.36
Zn (%)	n.d.	03.41

*n.d.=no decision

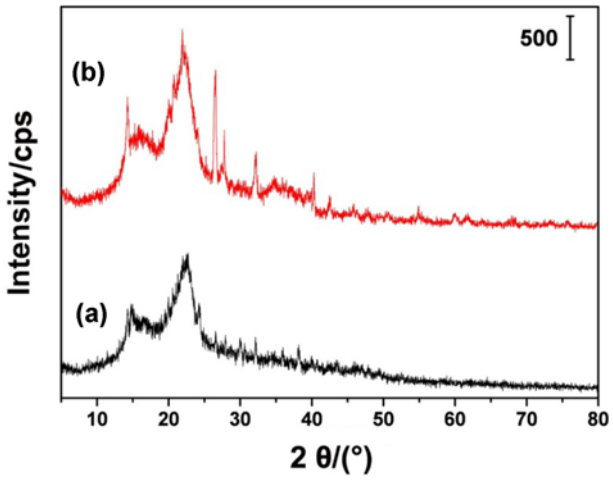

Fig. 8. X-ray of SSPO before (a) and after (b) Zn^{2+} biosorption (pH =6, temperature=30 °C, biomass dosage=1 g·L^{-1}, contact time=60 min, zinc initial concentration=150 mg·L^{-1}).

addition to increasing in height of the two broad peaks, which indicated that there were crystallines in the larger diffractive range of 15°-50°. It was probably that the SSPO shifted into metal compounds with crystalline structure. In comparison with XRD standards stored in JCPDF database of compounds, the pattern exhibited new peaks at around 2θ=14° and 22°, indicating the presence of $Zn_2PO_4(OH)$, at around 20° and 41° adding $(NH_4)_2Zn\cdot H_2O$ in major

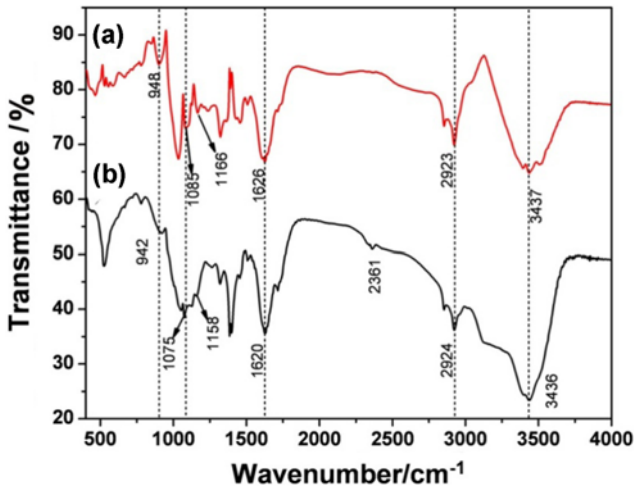

Fig. 9. FTIR Spectrometer of native (a) and metal-loaded (b) of SSPO (pH=6, temperature=30 °C, biomass dosage=1 g·L^{-1}, contact time=60 min, zinc initial concentration=150 mg·L^{-1}).

phase. Because of fewer peaks of ZnO at around 2θ=36° in minor phase, it was neglected in this study. Thus the XRD pattern provided strong evidence that there were complexation and coordination reactions between zinc ions and amino as well as phosphate group of SSPO, which is consistent with the results from SEM-EDX shown in Fig. 7.

6-4. FTIR Analysis of Adsorbents

The native and metal-loaded SSPO were also detected by FTIR in the range of 400-4,000 cm^{-1} shown in Fig. 9, to identify the functional groups of SSPO responsible for possible adsorbent-metal ion interactions. Each of the functional groups had its specific adsorption peaks. As shown in the figure, the spectra displayed a number of adsorption peaks, indicating the complex nature of the biomass examined. Relevant identified functional groups are listed in Table 3. The FTIR analysis of spectra indicated that the intense broad band around 3,437 cm^{-1} which shifted to 3,436 cm^{-1} may be due to the overlapping of O-H or N-H stretching vibration [40]. Chen et al. [41] reported that the formation of surface complexes can affect the peak position of -OH. The band shifted from 2,923 cm^{-1} to 2,924 cm^{-1} after biosorption may be relevant to C-H stretching vibration or the increasing preparation temperature, indicating a loss of the functional group C-H in the carbon prepared at higher temperature [42]. A new band at wave number 2,361 cm^{-1} with metal-loaded SSPO was probably the cumulative bond of ammonium salts attached

Table 3. General peak assignments of FTIR spectra biosorption bands of SSPO [37,38]

Wavenumber/cm^{-1}	Before biosorption	After biosorption	Difference	Functional groups
3200-3600	3437	3436	−1	-OH, -NH
2700-2950	2923	2924	+1	C-H
2360-2364	Absent	2361	-	$-NH_2$, -H
1400-1660	1626	1620	−6	C=O, C-N
1160-1420	1166	1158	−8	-OH, P=O
1000-1300	1085	1075	−10	C-O-C, C-O
690-990	948	942	−6	C-N, P-OH

to polyphenols or straight organic chains of biomass [43], indicating that it was probably involved with biosorption of zinc ions. The band around 1,626 cm^{-1} shifted to 1,620 cm^{-1} may be related to amide bond in the N-acetyl glucosamine polymer of the protein or the asymmetric and symmetric COO^- of deprotonated carboxylate functional groups of cellulose [44,45]. The band observed at 1,166 cm^{-1} and 948 cm^{-1} changed to 1,158 cm^{-1} and 942 cm^{-1} respectively, was assigned to P=O and P-OH stretching, which was considered to be indicative of phosphonate group [46]. Additionally, the change at 1,166 cm^{-1} also may due to N-H banding in amide , C=O stretching in carbonyl or amide band [47]. The change of band from 1,085 cm^{-1} to 1,075 cm^{-1} may correspond to C-O band of polysaccharides or C-O-C groups from β-(1-4)-glycosidic bonds in cellulose [48]. In summary, the bio-chemical reaction on SSPO surface changed chemical environment of functional groups to shift the corresponding bands. These spectra results offered additional evidence for biosorption mechanism of SSPO. The peak intensity on the spectrum suggested that functional groups of hydroxide, alkane, amide, phosphate, carboxyl, etc. were major contributors in metal ion uptake in agreement with ion exchange, complexation and coordination reaction.

6-5. Desorption Studies

The regeneration of the spent biomass and the recovery of metal ions are serious issues in practical applications. With 0.1 M HCl solution as eluent, more than 95% of the adsorbed zinc ions were desorbed from the biomass. To detect the reusability of the adsorbent, biosorption-desorption cycles were repeated five times by using the same conditions. After the first round of desorption, about 10% of the biosorption capacity was lost and this remained constant for all other cycles.

CONCLUSIONS

One of the agricultural by-products SSPO was used to remove Zn^{2+} from aqueous solution. The maximum biosorption capacity of zinc ions onto SSPO could reach above 50 $mg \cdot g^{-1}$, which was obtained at pH 6-7 with 150 $mg \cdot L^{-1}$ of Zn^{2+} initial concentration. The ionic strength has little influence on biosorption. The experimental data were well mathematically described by Langmuir model linear form and Freundlich model for non-linear form, indicating that monolayer adsorption on the surface of the adsorbent played an important role in biosorption and the SSPO is a favorable adsorbent. The biomass has a larger surface area with 51.16 m^2g^{-1}. Ion exchange, complexation and coordination reaction could participate in biosorption via SEM-EDX, XRD and FTIR analysis, and hydroxy, amide, phosphate, carboxyl, etc. were the critical functional groups in biochemical reaction. The unmodified SSPO also can be repeatedly used in adsorption process. So, SSPO without any chemical modification can be effective for elimination of zinc ion from effluents in terms of low-cost, abundant, high adsorption capacity and eco-friendly, possessing great potential for application.

ACKNOWLEDGEMENT

XiaoJing Hu and LiLong Yan contributed equally to this work. And this work is supported by the Special Scientific Fund for Nonprofit Environmental Industry (No. 2010467038).

REFERENCES

1. M. F. Ahmad, S. Haydar and T. A. Quraishi, *Int. Biodeterior. Biodegrad.*, **83**, 119 (2013).
2. S. Megateli, S. Semsari and M. Couderchet, *Ecotoxicol. Environ. Saf.*, **72**, 1774 (2009).
3. A. A. Juwarkar, S. K. Singh and A. Mudhoo, *Rev. Environ. Sci. Biotechnol.*, **9**, 215 (2010).
4. P. S. Vankar, R. Sarswat, A. K. Dwivedi and R. S. Sahu, *J. Clean. Prod.*, **60**, 65 (2013).
5. J. L. Wang and C. Chen, *Biotechnol. Adv.*, **27**, 195 (2009).
6. H. N. Bhatti, R. Khalid and M. A. Hanif, *Chem. Eng. J.*, **148**, 434 (2009).
7. A. Buasri, N. Chaiyut, K Tapang, S. Jaroensin and S. Panphrom, *APCBEE Procedia*, **3**, 60 (2012).
8. A. M. Abdel-Aty, N. S. Ammar, H. H. A. Ghafar amd R. K. Ali, *J. Adv. Res.*, **4**, 367 (2013).
9. C. W. Phan and V. Sabaratnam, *Appl. Microbiol. Biot.*, **96**, 863 (2012).
10. C. C. Tay, H. H. Liew, C. Y. Yin, S. A. Talib, S. Surif, A. A. Suhaimi and S. K. Yong, *Korean J. Chem. Eng.*, **28**, 825 (2011).
11. M. Arshad, M. N. Zafar, S. Younis and R. Nadeem, *J. Hazard. Mater.*, **157**, 534 (2008).
12. T. Altun and E. Pehlivan, *Food Chem.*, **132**, 697 (2012).
13. J. Rivera-Utrilla, I. Bautista-Toledo, M. A. Ferro-García and C. Moreno-Castilla, *J. Chem. Technol. Biotechnol.*, **76**, 1209 (2001).
14. W. S. Wan Ngah and M. A. K. M. Hanafiah, *Biochem. Eng. J.*, **39**, 521 (2008).
15. H. Li, Y. B. Lin, W. M. Guan, J. L. Chang, L. Xu, J. K. Guo and G. H. Wei, *J. Hazard. Mater.*, **179**, 151 (2010).
16. F. Martin-Dupont, V. Gloaguen, M. Guilloton, R. Granet and P. Krausz, *J. Environ. Sci. Heal. A.*, **41**, 149 (2006).
17. Y. Zhang, Y. F. Li, L. Q. Yang, X. J. Ma, L. Y. Wang and Z. F. Ye, *J. Hazard. Mater.*, **178**, 1046 (2010).
18. T. H. Shek, A. Ma, V. K. C. Lee and G. Mckay, *Chem. Eng. J.*, **146**, 63 (2009).
19. U. A. Guler and M. Sarioglu, *J. Environ. Chem. Eng.*, **1**, 369 (2013).
20. J. E. B. Cayllahua and M. L. Torem, *Chem. Eng. J.*, **161**, 1 (2010).
21. E. Malkoc, *J. Hazard. Mater.*, **137**, 899 (2006).
22. P. King, K. Anuradha, S. B. Lahari, Y. P. Kumar and V. S. R. K. Prasad, *J. Hazard. Mater.*, **153**, 324 (2008).
23. F. Çolak, N. Atar and A. Olgun, *Chem. Eng. J.*, **150**, 122 (2009).
24. I. Langmuir, *J .Am. Chem. Soc.*, **40**, 1361 (1918).
25. M. M. Areco, L. Saleh-Medina, M. A. Trinelli, J. L. Marco-Brown and M. dos S. Afonso, *Colloids Surf., B.*, **110**, 305 (2013).
26. G. Chen, G. M. Zeng, L. Tang, C. Du, X. Y. Jiang, G. H. Huang, H. Liu and G. Shen, *Bioresour. Technol.*, **99**, 7034 (2008).
27. L. K. Koopal, W. H. van Riemsdijk and J. C. M. de Wit, *J. Colloid Interface Sci.*, **166**, 51 (1994).
28. H. Freundlich, *Phys. Chem. Soc.*, **57**, 384 (1906).
29. M. Salman, M. Athar, U. Farooq, H. Nazir, A. Noor and S. Nazir, *Korean J. Chem. Eng.*, **30**, 1257 (2013).
30. H. Seo, M. Lee and S. Wang, *Environ. Eng. Res.*, **18**, 45 (2013).
31. T. Mathialagan, T. Viraraghavan and D. Cullimore, *Water Qual. Res. J. Canada*, **38**, 499 (2003).
32. V. Vinodhini and Nilanjana Das, *Desalination*, **264**, 9 (2010).
33. N. S. Kumar and M. Kim, *Chem. Eng. J.*, **168**, 562 (2011).

34. F. Gorzin and A. Asghar Ghoreyshi, *Korean J. Chem. Eng.*, **30**, 1594 (2013).
35. X. M. Li, Y. R. Tang, Z. X. Xuan, Y. H. Liu and F. Luo, *Sep. Purif. Technol.*, **155**, 69 (2007).
36. A. B. Albadarin, A. H. Al-Muhtaseb, N. A. Al-laqtah, G. M. Walker, S. J. Allen and M. N. M. Ahmad, *Chem. Eng. J.*, **169**, 20 (2011).
37. S. T. Akar, D. Arslan and T. Alp, *J. Hazard. Mater.*, **227-228**, 107 (2012).
38. V. O. Arief, K. Trilestar, J. Sunarso, N. Indraswati and S. Ismadji, *Clean*, **36**, 937 (2008).
39. M. A. Wahab, S. Jellali and N. Jedidi, *Bioresour. Technol.*, **101**, 5070 (2010).
40. G. C. Panda, S. K. Das and A. K. Guha, *Colloids Surf., B.*, **62**, 173 (2008).
41. H. Chen, G. L. Dai, J. Zhao, A. Zhong, J. Wu and H. Yan, *J. Hazard. Mater.*, **177**, 228 (2010).
42. J. H. Zhang, H. Fu, X. S. Lv, J. Tang and X. H. Xu, *Biomass Bioenergy*, **35**, 464 (2011).
43. V. Sarin, T. S. Singh and K. K. Pant, *Bioresour. Technol.*, **97**, 1986 (2006).
44. A. Javaid, R. Bajwa, U. Shafique and J. Anwar, *Biomass Bioenergy*, **35**, 1675 (2011).
45. M. A. Wahab, H. Boubakri, S. Jellali and N. Jedidi, *J. Hazard. Mater.*, **241-242**, 101 (2012).
46. F. Pagnanelli, M. P. Papini, L. Toro, M. Trifoni and F. Veglio, *Environ. Sci. Technol.*, **34**, 2773 (2000).
47. L. Ramrakhiani, R. Majumder and S. Khowala, *Chem. Eng. J.*, **171**, 1060 (2011).
48. D. M. Suflet, G. C. Chitanu and V. I. Popa, *React. Funct. Polym.*, **66**, 1240 (2006).